Production of halo particles by excitation of collective modes in high-intensity charged particle beams

Sean Strasburg and Ronald C. Davidson
Plasma Physics Laboratory, Princeton University, Princeton, New Jersey 08543
(Received 14 June 1999)

This paper examines analytically and numerically the effects of self-consistent collective oscillations excited in a high-intensity charged particle beam on the motion of a test particle in the beam core. Even under ideal conditions, assuming a constant transverse focusing force (smooth focusing approximation), and perturbations about a uniform-density, constant radius beam, it is found that collective mode excitations, in combination with the applied focusing force and the equilibrium test fields, can eject particles from the beam core to large radii. Test particle orbits are calculated for collective oscillations with $n=1$ and 2 radial mode structure, and an estimate is obtained for the range of initial conditions for which particles will be expelled from the beam interior. Resonances for meridional particles are found to be unimportant, while a class of particles with nonzero angular momentum are found to participate in resonant behavior. Once expelled from the beam, numerical solutions of the orbit equations indicate that Kolmogorov-Arnold-Moser curves, phase space spanning integrals of motion, confine particles within 1.5 times the beam radius for moderately low mode amplitudes, but are successively destabilized for higher amplitudes.

PACS number(s): 29.27.−a

I. INTRODUCTION

It is increasingly important to develop improved theoretical models of halo production and control for charged particle beam propagation in high-intensity accelerators and transport systems [1,2], with applications to spallation neutron sources, heavy ion fusion, nuclear waste treatment, and tritium production. Halo formation mechanisms, such as beam mismatch and nonlinearities associated with nonuniform space-charge forces, have been explored both analytically and numerically [3,4].

The core-particle model of Gluckstern [5] was an early, successful attempt to describe the structure of the halo generated by perturbing the beam about an rms-matched equilibrium, leading to an envelope mismatch oscillation. This method simplified the dynamics by averaging over terms away from a 2:1 parametric resonance, creating an integral of the motion. This integral was used to describe the particle behavior, and the predictions of halo structure closely resembled numerical simulations. This averaging procedure, however, also eliminated chaotic and diffusive elements of the trajectories. In addition, since initial conditions had to be chosen placing particles outside the beam surface, the model did not describe the self-consistent expulsion of particles from the beam core.

The analysis of envelope instabilities by Gluckstern [6] described regions in parameter space in which the amplitude of the breathing mode of the beam core would grow in time. This could lead to particles being expelled from the beam, but it required a gross instability which may not be present in practical applications or may saturate at a low level. It did not attempt to explain how quasisteady conditions could result in particles leaving the beam.

The idea of collimation [7] is highly relevant to attempts to keep expelled particles away from the machine structure. It relies, however, on several important assumptions. The distinction between halo and core particles must be predominantly preserved over time, so that halo particles should stay removed from the beam core in phase space [8,9], and not cycle in and out of the beam [10]. Methods of particle expulsion not explicitly included in the model must function sufficiently slowly that collimation is effective and does not unacceptably diminish the beam brightness.

Many recent numerical simulations have studied the effects of mismatch oscillations. Pakter and Chen [11] have found with extensive test particle simulations that Kolmogorov-Arnold Moser (KAM) surfaces persist outside mismatched periodically focused Kapchinskij-Vladimirskij beams for significant envelope oscillation amplitudes. Okamoto and Ikegami [9] briefly discuss the possibility of a stochastic instability in the core tail—the edge of the beam in phase space—caused by static field nonlinearities in uniform-focusing channels. For such a time-independent case, however, motion inside the beam is regular due to the existence of a first integral.

Finally, the work of Qian and co-workers [12] and Fink, Chen, and Marable [13] showed that nonlinear space-charge forces in periodically focused channels are able to expel particles and excite them to significant radii. The static charge density profiles assumed in the model, however, are not self-consistent, since they are not solutions of the Vlasov-Poisson equations. Although this research built on expectations that distributions more complicated than the Kapchinskij-Vladimirskij distribution [14] would lead to a lack of particle confinement, it was not clear how rigorous the conclusions could be made.

Despite the significant advances noted above, a fundamental understanding of halo production is incomplete. In this paper, we consider a mechanism for the production of halo particles. Namely, we consider the effects of self-consistent collective oscillations excited in a high-intensity

ion beam on the motion of a test particle in the beam core. Even under ideal conditions, assuming a constant transverse focusing force (smooth focusing approximation), and perturbations about a uniform-density, constant-radius beam, it is found that collective mode excitations, in combination with the applied focusing force and the equilibrium self fields, can eject particles from the beam core to large radii.

In Sec. II we present the assumptions which underlie the theoretical model for the beam equilibrium and perturbative modes. This allows us to develop test particle equations in Sec. II C, which are then analyzed theoretically in Sec. III, including resonant (Sec. III A) and nonresonant (Sec. III B) behavior for particles initially in the beam interior. For extended dynamics of particles traveling both in the interior and exterior regions, we discuss numerical results in Sec. IV. Improvements to the analytical estimates are made in Sec. IV B, and the maximum excursion of particles out of the beam is determined in Sec. IV C.

II. THEORETICAL MODEL AND ASSUMPTIONS

A. Equilibrium

We consider an intense nonneutral ion beam with beam radius R propagating in the z direction. The characteristic axial momentum of a beam particle is $\gamma_b m\beta_b c$, where $V_b=\beta_b c=$const is the directed axial velocity. Here, m is the ion rest mass, c is the speed of light in vacuo, $\gamma_b=(1-\beta_b^2)^{-1/2}$ is the relativistic mass factor, and the ion charge is denoted by $+Ze$. In the present analysis, the applied transverse focusing force is modeled in the smooth focusing approximation by

$$\mathbf{F}_{foc}(\mathbf{x})=-\gamma_b m\omega_f^2(x\hat{\mathbf{e}}_x+y\hat{\mathbf{e}}_y), \tag{1}$$

where ω_f is a constant focusing frequency with units of inverse time. Here, $\mathbf{x}$ is the vector position, $\mathbf{x}=(x,y)$, related to the scalar radial distance from the beam axis, r, by $r=(x^2+y^2)^{1/2}$. The transverse displacement from the beam axis is (x,y). The effects of self-electric and self-magnetic fields on the particle dynamics are retained in a self-consistent manner, consistent with the paraxial approximation, and the assumption that Budker's parameter, ν_B, is much less than the relativistic mass factor, $\nu_B=N_b(Ze)^2/mc^2\ll\gamma_b$. Here N_b is the number of beam ions per unit axial length, related to the number density of beam ions $n_b(x,y,t)$, the number of particles per unit volume, by $N_b=\int dx\,dy\,n_b$.

The assumptions of constant axial beam velocity V_b and paraxiality allow us to convert from units of time to axial length s through $s=\beta_b ct$. The wave number equivalent to the transverse focusing frequency, the transverse focusing coefficient κ, is defined by $\sqrt{\kappa}=\omega_f/\beta_b c$, which has units of inverse length. Beam quantities such as $n_b(x,y,t)$ will be expressed as $n_b(x,y,s)$ through this conversion, and derivatives $(\cdot)'$ will refer to spatial derivatives, $d/ds(\cdot)$. Since they are equivalent, we will refer to frequency and wave number interchangeably. We further assume axisymmetric unbunched beam propagation $(\partial/\partial\theta=0=\partial/\partial z)$, and introduce the normalized dimensionless self-field potential ψ defined by

$$\psi(r,s)=\frac{Ze}{\gamma_b^3 m\beta_b^2 c^2}\,\phi(r,s). \tag{2}$$

In Eq. (2), $r=(x^2+y^2)^{1/2}$ is the radial distance from the beam axis, and the space-charge potential $\phi(r,s)$ is determined self-consistently in terms of the density profile $n_b(r,s)$ from Poisson's equation, $r^{-1}(\partial/\partial r)[r\partial\phi/\partial r]=-4\pi Zen_b$. A perfectly conducting cylindrical wall is located at radius $r=r_w$, where the boundary conditions is $\phi(r=r_w,s)=$const.

We assume a kinetic [14] or warm-fluid [15] Kapchinksij-Vladimirskij beam equilibrium, and for this case the equilibrium density profile $n_b^0(r,s)$ is uniform in the beam interior with

$$n_b^0(r,s)=\begin{cases}\dfrac{N_b}{\pi R^2}, & 0\leq r<R(s);\\[2mm] 0, & R(s)<r\leq r_w.\end{cases} \tag{3}$$

In Eq. (3), N_b is constant, and $R(s)$ is the solution to the envelope equation [16],

$$\frac{d^2R}{ds^2}+\left(\kappa-\frac{K}{R^2}\right)R=\frac{\epsilon^2}{R^3}, \tag{4}$$

where $\kappa=\omega_f^2/\beta_b^2c^2$ is the transverse focusing coefficient, ϵ is the unnormalized transverse emittance, and K is the dimensionless self-field perveance defined by [14]

$$K=\frac{2N_b(Ze)^2}{\gamma_b^3 m(\beta_b c)^2}. \tag{5}$$

For our purposes here, we further assume a matched, constant-radius beam equilibrium with $R(s)=R_0$, a constant. The only explicit time dependence in the problem is therefore due to the eigenmode excitations, to be discussed below in Sec. II B. Using Eq. (4), R_0 is determined self-consistently in terms of κ, K, and ϵ^2 from Eq. (4)

$$\left(\kappa-\frac{K}{R_0^2}\right)R_0=\frac{\epsilon^2}{R_0^3}. \tag{6}$$

For the constant-radius, uniform-density beam consistent with Eqs. (3) and (6), it is readily shown that the equilibrium self-field potential $\psi_0(r)$ is parabolic in the beam interior, and logarithmic outside. We obtain from Eq. (3) and Poisson's equation

$$\psi_0=\begin{cases}-\dfrac{1}{2}K\bar{r}^2, & 0\leq\bar{r}<1,\\[2mm] -\dfrac{1}{2}K(1+2\ln\bar{r}), & 1<\bar{r}\leq\bar{r}_w.\end{cases} \tag{7}$$

Here, barred coordinates have been normalized by the constant beam radius R_0, so that $\bar{r}\equiv r/R_0$ and $\bar{r}_w\equiv r_w/R_0$. The boundary conditions set ψ_0 at the wall equal to the constant value $\psi_w=-(K/2)\,[1+2\ln\bar{r}_w]$.

In the beam interior, the external force $\mathbf{F}_{\rm foc}$ harmonically focuses the particle motion with undepressed wave number $\omega_0\equiv\sqrt{\kappa}$, while the self-field potential ψ_0 harmonically defo-

TABLE I. Normalized eigenmode potentials ψ_n and eigenfrequencies $\bar{\omega}_n^2$ for the infinite set of collective modes described in Sec. II B. The frequency $\bar{\omega}_n$ is normalized to the undepressed tune, $\bar{\omega}_n = \omega_n / \nu_0$.

Mode number	Normalized eigenmode potential ψ_n	Eigenfrequency $\bar{\omega}_n^2$
1	$1-\bar{r}^2$	$2+2\bar{\nu}^2$
2	$1-4\bar{r}^2+3\bar{r}^4$	$2+14\bar{\nu}^2$
3	$1-9\bar{r}^2+18\bar{r}^4-10\bar{r}^6$	$2+34\bar{\nu}^2$
4	$1-16\bar{r}^2+60\bar{r}^4-80\bar{r}^6+35\bar{r}^8$	$2+62\bar{\nu}^2$
5	$1-25\bar{r}^2+150\bar{r}^4-350\bar{r}^6+350\bar{r}^8-126\bar{r}^{10}$	$2+98\bar{\nu}^2$
n	$\frac{1}{2}[P_{n-1}(1-2\bar{r}^2)+P_n(1-2\bar{r}^2)]$	$2+2\bar{\nu}^2(2n^2-1)$

cuses with wave number $\sqrt{K/R_0^2}$. The ''depressed'' oscillation wave number $\bar{\nu}$ (dimensionless units) is defined in terms of the transverse focusing coefficient κ, perveance K, and equilibrium beam radius R_0 by

$$\bar{\nu}^2 = 1 - \frac{K}{\kappa R_0^2}. \tag{8}$$

The ''depressed'' oscillation wave number ω (dimensional units) is given by

$$\omega^2 = \kappa\bar{\nu}^2 = \kappa - \frac{K}{R_0^2} = \omega_0^2 - \frac{K}{R_0^2}. \tag{9}$$

B. Self-consistent perturbations

A key focus of the present analysis is to investigate the motion of a test ion in the combined fields of the applied focusing field in Eq. (1), the equilibrium self-field in Eq. (7), and the perturbed self-field associated with self-consistent collective oscillations excited in the beam.

We express the total self-field potential as

$$\psi(\bar{r},s) = \psi_0(\bar{r}) + \delta\psi(\bar{r},s), \tag{10}$$

where $\psi_0(\bar{r})$ is defined in Eq. (7) for the case of a step-function equilibrium density profile considered here. For the perturbed potential $\delta\psi(\bar{r},s)$, we make use of the warm-fluid model developed by Lund and Davidson [15]. This macroscopic model neglects the heat flow [$\nabla\cdot\mathbf{Q}\simeq 0$], but follows the self-consistent evolution of the beam density n_b, flow velocity $\mathbf{V}_b$, and pressure tensor $\mathbf{P}_b$. For perturbations about a warm-fluid equilibrium with step-function density profile [Eq. (3)], the analysis [15] predicts an infinite class of stable oscillations, each with its own eigenfrequency and radial eigenfunction. The perturbed potentials are polynomial in $\bar{r}^2$ in the beam interior (oscillating sinusoidally in time), and vanish outside the beam, i.e.,

$$\delta\psi^s = \begin{cases} \displaystyle\sum_{n=1}^{\infty} \delta\psi_n(\bar{r}^2)\cos(\omega_n s+\beta_n), & 0\leqslant\bar{r}<1, \\ 0, & 1<\bar{r}\leqslant\bar{r}_w. \end{cases} \tag{11}$$

Here, $\{\beta_n\}$ are constant phases. The radial eigenfunction $\delta\psi_n(\bar{r}^2)$ is defined in terms of the Legendre polynomials (of the first kind), $P_{n-1}(x)$ and $P_n(x)$, by

$$\delta\psi_n(\bar{r}^2) = \frac{A_n}{2}[P_{n-1}(1-2\bar{r}^2)+P_n(1-2\bar{r}^2)] \tag{12}$$

where $\{A_n\}$ are constant amplitudes. The normal-mode oscillation wave numbers $\{\omega_n\}$ are defined by $\omega_n^2=\kappa[2+2\bar{\nu}^2(2n^2-1)]$ in Ref. [15]. For completeness, the functional forms of the eigenmodes and the dispersion relations for low values of n are summarized in Table I.

A remarkable feature of the warm-fluid analysis is that the normal modes $\{\omega_n\}$ are in excellent agreement with the (stable) high-frequency oscillations calculated by Gluckstern [17] using a kinetic model based on the Vlasov-Poisson equations. This conclusion is valid over a wide range of values of the self-field perveance K [15].

In Eqs. (11) and (12), the dimensionless amplitudes $\{A_n\}$ are required to be small for the linearization to be valid. We choose to quantify this smallness by comparing the bulk rms electrostatic energy in the nth collective mode, $\mathcal{E}_n$, to that in the equilibrium electrostatic energy within the beam, $\mathcal{E}_0$. Electrostatic energy $\mathcal{E}$ is proportional to the square of the local self-electric field, $\mathcal{E}=|E|^2/8\pi=|\nabla\phi|^2/8\pi$. This is integrated over time and volume to obtain the bulk rms value. We obtain

$$8\pi\mathcal{E}_n = \frac{1}{T_n}\int_0^{T_n} dt\, 2\pi\int_0^{R_0}\left|\frac{\partial}{\partial r}\phi_n(r,t)\right|^2 r\,dr, \tag{13}$$

where $\phi_n(r,t)$ is the self-field potential of the nth mode, and T_n is its period. Furthermore, we express the dimensional expansion coefficients $\{A_n\}$ in Eq. (12) as $A_n=c_n e_n \delta_n K$, where K is the self-field perveance. Here, c_n is defined by

$$c_n^{-1} = -\left[2\frac{\partial}{\partial\bar{r}^2}\delta\psi_n(\bar{r}^2)\right]_{\bar{r}^2=0} \tag{14}$$

in order to normalize the coefficient of the $\bar{r}$ term in the oscillating polynomial to unity. In addition, e_n is chosen so as to make the criterion of smallness—that the mode's energy be small compared to the beam's—take the nondimensional form that some small parameter, δ_n^2 be much smaller than unity, as follows.

We find for the harmonic potential generated by the equilibrium step-function density profile that

$$\mathcal{E}_0 = \alpha^2\frac{R_o^4}{4}, \tag{15}$$

where $\alpha=(Ze\pi n_b^0)^2$ and $n_b^0=N_b/\pi R_0^2$ is the constant number density of the flat-top beam. For the $n=1$ collective mode, the definition of $c_1=1/2$, and we find that

$$\mathcal{E}_1=\delta_1^2\alpha^2\frac{e_1}{2}\frac{R_0^4}{4}. \tag{16}$$

Comparing Eqs. (16) and (15), the condition that $\mathcal{E}_1/\mathcal{E}_0\ll 1$ be equivalent to $\delta_1^2\ll 1$ requires that $e_1=2$. Similarly, for the $n=2$ mode, $c_2=1/8$, and $\mathcal{E}_2=\delta_2^2 e_2 R_0^4/64$, and so $e_2=16$. If we denote the ratio of mode energy to beam energy $\Gamma_n=\delta_n^2$, the definition of c_n and e_n together make the condition that the rms electrostatic energy in the nth collective mode is small compared to the beam's field energy reduce to

$$\delta_n^2\ll 1. \tag{17}$$

C. Test ion orbit equations

We consider the motion of an individual test ion in the axisymmetric field configuration described by Eqs. (1) and (10). Because $\partial/\partial\theta=0$ is assumed, the (normalized) canonical angular momentum $\overline{P}_\theta=P_\theta/\gamma_b m\beta_b c R_0^2$ is conserved, i.e.,

$$R_0^2\overline{P}_\theta=x\frac{dy}{ds}-y\frac{dx}{ds}=\text{const.} \tag{18}$$

Furthermore, it is readily shown that the equation of motion for the normalized radial coordinate $\overline{r}(s)=r(s)/R_0$ of the test ion is given by

$$\frac{d^2\overline{r}}{ds^2}+\left(\kappa+\frac{2}{R_0^2}\frac{\partial\psi}{\partial\overline{r}^2}\right)\overline{r}=\frac{\overline{P}_\theta^2}{\overline{r}^3}. \tag{19}$$

In this equation, $\kappa=\omega_f^2/\beta_b^2c^2$ is the transverse focusing parameter, and $\psi(\overline{r},s)=\psi_0(\overline{r})+\delta\psi(\overline{r},s)$ is defined in Eqs. (7) and (11). Equation (19) is a valid description of the test ion motion, both inside the beam ($\overline{r}<1$) and outside the beam ($\overline{r}>1$).

Finally, we shall assume, unless otherwise stated, that the analysis is restricted to particle orbits that pass through the beam axis $(x,y)=(0,0)$, and thus have zero angular momentum. (We call these particles *meridional*.) For example, setting $y(s=0)=0=(dy/ds)_{s=0}$ gives $\overline{P}_\theta=0$, and the orbit equation for $\overline{x}(s)=x(s)/R_0$ reduces to motion in the x plane:

$$\frac{d^2\overline{x}}{ds^2}+\left[\kappa+\frac{2}{R_0^2}\left(\frac{\partial\psi}{\partial\overline{r}^2}\right)_{\overline{r}=\overline{x}}\right]\overline{x}=0. \tag{20}$$

For test-particle motion including angular momentum inside the beam ($\overline{r}<1$), we obtain by substituting the equilibrium and perturbed self-field potentials

$$\frac{d^2\overline{r}}{ds^2}+\left[\kappa-\frac{K}{R_0^2}\right]\overline{r}-\frac{\overline{P}_\theta^2}{\overline{r}^3}=\frac{K}{R_0^2}\sum_{n=1}^{\infty}\delta_n c_n e_n\frac{\partial}{\partial\overline{r}}\delta\psi_n(\overline{r})\cos\times(\omega_n s+\beta_n), \tag{21}$$

where use has been made of $A_n=c_n e_n\delta_n K$, and c_n is defined in Eq. (14) and by the requirement Eq. (17). Similarly, for meridional motion inside the beam ($|\overline{x}|<1$) we obtain

$$\frac{d^2\overline{x}}{ds^2}+\left[\kappa-\frac{K}{R_0^2}\right]\overline{x}=\frac{K}{R_0^2}\sum_{n=1}^{\infty}\delta_n c_n e_n\frac{\partial}{\partial\overline{x}}\delta\psi_n(\overline{x})\cos(\omega_n s+\beta_n). \tag{22}$$

We also recall the relation between the undepressed wave number, $\omega_0=\sqrt{\kappa}$, and the space-charge-depressed wave number, ω,

$$\omega^2=\omega_0^2-\frac{K}{R_0^2}=\kappa-\frac{K}{R_0^2}, \tag{23}$$

in order to write the left-hand side of Eq. (22) as $\overline{x}''+\omega^2\overline{x}$. For comparison, for $\overline{P}_\theta^2=0$ the equation to be solved for particle motion in the interior of a mismatched beam is

$$\frac{d^2\overline{x}}{ds^2}+\left(\kappa-\frac{K}{R^2(s)}\right)\overline{x}=0, \tag{24}$$

where $R(s)$ is obtained by solving Eq. (4). On the other hand, for $\overline{P}_\theta^2\neq 0$, particle motion outside the beam ($\overline{r}>1$), Eq. (20) reduces to the nonlinear autonomous equation

$$\frac{d^2\overline{r}}{ds^2}+\left(\kappa-\frac{K}{R_0^2\overline{r}^2}\right)\overline{r}-\frac{\overline{P}_\theta^2}{\overline{r}^3}=0, \tag{25}$$

where use has been made of Eqs. (20), (7), and (11), and to

$$\frac{d^2\overline{x}}{ds^2}+\left(\kappa-\frac{K}{R_0^2\overline{x}^2}\right)\overline{x}=0 \tag{26}$$

for $\overline{P}_\theta^2=0$ and $|\overline{x}|>1$.

Equations (22) and (26), supplemented by the associated definitions of $\delta\psi_n$, $\{\omega_n\}$, etc., constitute the final form of the test-particle orbit equations to be investigated analytically and numerically in Secs. III and IV.

III. THEORY OF THE DYNAMICAL SYSTEMS

In this section we examine several features of the test ion motion analytically, using numerical solutions as verification.

There are two ways for a particle which would normally be confined within the beam to leave the beam interior and sample the highly nonlinear exterior region. A particle which would remain in the interior in the unperturbed case—and thus be governed exclusively by the interior dynamics—may either resonantly gain energy from the perturbation, with the possibility of large excursions, or nonresonantly absorb and then give back energy.

In the *resonant* case, the gain in energy is limited by the tendency to fall out of resonance, and by the change in dynamics when the particle finally exits the beam core. However, the nature of the flat-top density profile in Eq. (3) makes it easy for particles to stay in resonance until they leave the beam. Since the unperturbed beam generates harmonic motion for meridional particles in the interior, the tunes of particles with different energies do not differ, pro-

vided the particle remains confined. In addition, since the fluid modes have purely oscillating perturbations, they do not cause a higher-order tune shift. Thus, if a fluid mode resonance is encountered, it will affect all meridional particles in the beam.

In the *nonresonant* case, while the gain in energy is small, it may be enough to push particles over the ''tune edge'' at the beam radius R_0. If a particle temporarily picks up energy, but is ejected from the beam core in the process, the new dynamical system may prevent it from simply giving the energy back and executing small oscillations around its unperturbed orbit.

Although a complete solution to the full problem demands that two dynamical regimes—interior and exterior to the beam—be connected smoothly together, the question of whether particles which normally would be confined can escape at all can be answered by simply noting under what conditions advancing the particle motion in the interior dynamical system forward causes particles to leave the beam.

A. Resonant behavior

1. n=1 mode for meridional test ions

We begin by considering a beam supporting only an $n=1$ mode. The normalized potential for this mode is $\psi_1 = A_1(1-\overline{x}^2)$, where the amplitude coefficient $A_n=\delta_1$. Using this potential in Eq. (21), we find for motion inside the beam,

$$\frac{d^2\overline{r}}{ds^2}+\left(\kappa-\frac{K}{R_0^2}\right)\overline{r}-\frac{\overline{P}_\theta^2}{\overline{r}^3}-\frac{K}{R_0^2}\,\delta_1\overline{r}\cos(\omega_1 s+\beta_1)=0. \tag{27}$$

Equation (27) can be further reduced, using the definition $\omega^2=\omega_0^2-K/R_0^2$ in Eq. (9), and setting the arbitrary phase β_1 equal to zero. In addition, we assume meridional particles; i.e., $\overline{P}_\theta^2=0$. This gives the equation

$$\frac{d^2\overline{x}}{ds^2}+\omega^2\overline{x}-\delta_1(\omega_0^2-\omega^2)\overline{x}\cos\omega_1 s=0. \tag{28}$$

This is a Mathieu equation [18] of the form

$$\frac{d^2y}{dt^2}+(\omega^2+\delta\cos\omega_\delta t)y=0, \tag{29}$$

with well-known resonances near $\omega_\delta/\omega=1$ (fundamental resonance) and $\omega_\delta/\omega=2$ (principal, or Mathieu resonance). In our case, it is seen from Table I that ω_1 is given by $\omega_1^2=2\omega_0^2(1+\overline{\nu}^2)$.

It is illuminating to compare Eq. (28) with the equation for a small envelope oscillation. Rather than taking $R=R_0=\text{const}$ in Eq. (4), we assume $R(s)=R_0(1+1/2\delta_e\cos\omega_e s)$. The envelope oscillation frequency for this small-amplitude mismatch mode is given by $\omega_e^2=2\omega_0^2(1+\overline{\nu}^2)$, which is the same as the frequency ω_1 for the $n=1$ collective mode. If we replace K/R_0^2 by $K/R^2(s)$ in the orbit equation for $\overline{x}(s)$ in the beam interior $(-1<\overline{x}<1)$, we obtain Eq. (24). Linearizing for small δ_e taking $\delta\psi=0$, this equation becomes

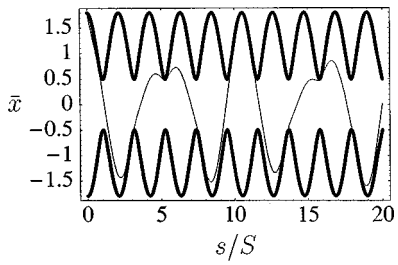

FIG. 1. Test ion trajectory (light line) in a beam (dark line) launched at 1.8 times the rms-matched value $R_{\rm rms}$. The test ion was initially just inside the beam edge. The space-charge depression factor is $\overline{\nu}^2=1/3$.

$$\frac{d^2\overline{x}}{ds^2}+\omega^2\overline{x}-\delta_e(\omega_0^2-\omega^2)\overline{x}\cos\omega_e s=0. \tag{30}$$

Taking $\delta_e=\delta_1$, Eqs. (28) and (30) are identical. For meridional motion outside the beam the orbit equations for the $n=1$ mode and the envelope mismatch mode are also the same, i.e.,

$$\frac{d^2\overline{x}}{ds^2}+\left(\kappa-\frac{K}{R_0^2\overline{x}^2}\right)\overline{x}=0. \tag{31}$$

However, it is important to distinguish what constitutes *outside* the beam for the two cases. The fluid modes are derived for perturbations about a constant radius beam, so *outside the beam* corresponds to $|\overline{x}|>1$, or $|x|>R_0$. The mismatch ripple, however, requires $|x|>R(s)=R_0(1+1/2\delta_e\cos\omega_e s)$. This distinction has practical consequences. We shall neglect resonances for the moment. In both the mismatch case and the $n=1$ case, the test particle equation is a time-modulated harmonic oscillator, and, unless a Mathieu resonance is encountered, tori are therefore invariant.

In the case of a *mismatched* beam with no other collective perturbations, if a meridional test particle is launched at the beam edge with the same radial velocity as the beam envelope—or with any energy less than this—the equation of motion predicts that it will remain confined for all time. In the case of an envelope mismatch, the envelope $R(s)$ is itself the projection of an energy level [2] onto the x axis. That is, the stability of the beam envelope, which itself corresponds to maximal-radius particle trajectories, guarantees the *stability and confinement* of particle orbits under an envelope mismatch. Therefore, the projected phase space trajectory which yields the beam radius $R(s)$ cannot be crossed except by resonant breaking of tori, and all particles initially within the beam remain confined in the beam interior. Figure 1 shows the motion of a particle with energy slightly below that needed to escape the beam core.

For a constant radius beam supporting a *collective mode*, however, the beam edge R_0 is not the projection of an energy level. The self-field potential caused by the modes do not, in general, have nodes at $r=R_0$, and so the energy associated with the beam edge oscillates in time. Since particles that would normally be inside a mismatched beam might be outside a beam supporting an $n=1$ collective mode, experiencing the exterior nonlinear forces, there is no guarantee of invariant tori. That is, since the equations of motion for a linearized mismatch and the $n=1$ mode are identical, *stabil-*

ity of particle orbits inside the beam is also guaranteed by the stability of the envelope, but confinement is not guaranteed, since particles may sample the exterior region under the influence of an $n=1$ mode when they would not in a mismatched beam. If the particle in Fig. 1 were inside a beam supporting an $n=1$ mode and not a mismatch oscillation mode, the particle would in fact escape from the $R=$const. beam. In practice, particles near the edge escape the beam and experience significant energy changes. This behavior is treated further in Sec. III B.

Returning to examining resonant behavior, we reiterate the impossibility of encountering the Mathieu resonances near $\omega_1=2\omega$. As the test particle trajectories begin to come into resonance with the Mathieu mode, the resonance strength approaches zero [19]. Heuristically, this can be seen more clearly by normalizing the depressed frequency to unity in either the mismatch equation or the $n=1$ equation so that there is only one normalized frequency in the problem. We introduce a new scaled time $\bar{s}=\omega s$. Thus Eq. (28) transforms into

$$\frac{d^2\bar{x}}{d\bar{s}^2}+\bar{x}-\delta_1\frac{\omega_0^2-\omega^2}{\omega^2}\bar{x}\cos\left(\frac{\omega_1}{\omega}\bar{s}\right)=0. \tag{32}$$

Using the fact that $\omega^2=\bar{\nu}^2\omega_0^2$, and that

$$\frac{\omega_1^2}{\omega^2}=\frac{2\omega_0^2(1+\bar{\nu}^2)}{\omega_0^2\bar{\nu}^2}, \tag{33}$$

we obtain

$$\frac{d^2\bar{x}}{d\bar{s}^2}+\bar{x}-\delta_1\frac{1-\bar{\nu}^2}{\bar{\nu}^2}\bar{x}\cos\left(\bar{s}\sqrt{2+\frac{2}{\bar{\nu}^2}}\right)=0. \tag{34}$$

Thus, when the time-dependent term in Eq. (34) term approaches $\cos 2\bar{s}$ as $\bar{\nu}\to 1$, the mode coefficient proportional to $1-\bar{\nu}^2$ approaches zero. The particle trajectories as $\bar{\nu}\to 1$ are confirmed numerically to be well behaved.

Hence, we can conclude that there are no important resonances for a meridional particle inside a beam supporting an $n=1$ collective mode.

2. n=2 mode for meridional test ions

The $\bar{x}^3$ dependence of the $n=2$ mode (see Table I) raises the possibility of a nonlinear parametric resonance. We will find that, although resonances would exist if the depressed frequency and the second mode eigenfrequency could be varied independently, they are ''inaccessible'' due to the functional relationship between ω and ω_2.

The equation of motion for a test particle with general value of canonical angular momentum $\bar{P}_\theta$ in a beam supporting an $n=2$ collective mode is (for $\bar{r}<1$)

$$\frac{d^2\bar{r}}{ds^2}+\left(\kappa-\frac{K}{R_0^2}\right)\bar{r}-\frac{\bar{P}_\theta^2}{\bar{r}^3}-\delta_2\frac{K}{R_0^2}\left(\bar{r}-\frac{3}{2}\bar{r}^3\right)\cos(\omega^2 s+\beta_2)=0. \tag{35}$$

Note that the parametric term proportional to δ_2 vanishes when, during the test ion's trajectory, the condition

$$\bar{r}=\sqrt{2/3} \tag{36}$$

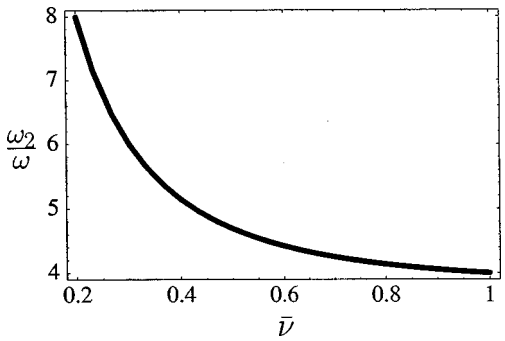

FIG. 2. Plot of the ratio of $n=2$ collective mode frequency to the depressed transverse particle frequency, ω_2/ω, as a function of space-charge depression factor ν.

is satisfied: we will examine this issue in Sec. II B. We convert the coefficients in Eq. (35) to wave numbers, choose the arbitrary phase β_2 to be zero, and consider only meridional test ions ($\bar{P}_\theta^2=0$), changing $\bar{r}$ to $\bar{x}$. The Hamiltonian $H(\bar{x},\bar{p},s)$ describing the motion in Eq. (35) under these conditions is given by (for $|\bar{x}|<1$)

$$H=\frac{1}{2}\bar{p}^2+\frac{1}{2}\omega^2\bar{x}^2-\delta_2(\omega_0^2-\omega^2)\left(\frac{1}{2}\bar{x}^2-\frac{3}{8}\bar{x}^4\right)\cos\omega^2 s, \tag{37}$$

where $\bar{p}$ denotes $d\bar{x}/ds$. From this Hamiltonian, it appears that the principal resonances for cubic nonlinearities in parametric equations are at $\omega_2/\omega=\pm 2,\pm 4$. This claim will be verified below in Sec. III B. Referring to Table I, we find that

$$\frac{\omega_2^2}{\omega^2}=\frac{2(1+7\bar{\nu}^2)}{\bar{\nu}^2}. \tag{38}$$

A plot of ω_2/ω is presented in Fig. 2. From this it is clear that, over the entire range of space-charge depression, the ratio ω_2/ω never approaches the values of 2 or 4.

Therefore, fundamental and principal resonances are not expected to be important for the $n=2$ collective mode.

3. Higher-order modes

In fact, the functional relationship between the nth mode frequency ω_n and the depressed transverse frequency ω makes these principal resonances inaccessible for all mode numbers n. The Hamiltonian expansions predict resonances for the nth mode at $\omega_n/\omega=\pm 2m$ for integers $m\leqslant n$. Using the dispersion relation in Table I, we obtain

$$\frac{\omega_n^2}{\omega^2}=\frac{2+2\bar{\nu}^2(2n^2-1)}{\bar{\nu}^2}\doteq g_n(\bar{\nu}^2). \tag{39}$$

Defining $\bar{n}=2n^2-1$ and denoting $u=\bar{\nu}^2$, we find for the first two derivatives of $g_n(u)=2(1+\bar{n}u)/u$,

$$\frac{dg_n(u)}{du}=\frac{-2}{u^3}(1+\bar{n}u)+\frac{2}{u}\bar{n},$$
$$\frac{d^2g_n(u)}{du^2}=\frac{4}{u^3}. \tag{40}$$

Setting the first derivative equal to zero yields the contradiction $1+\bar{n}u=\bar{n}x$, and so the only extrema are on the boundary points $u=0,1$. Since the second derivative is positive in this region, the minimum occurs at $u=1$, and from Eq. (39), $g_n(u)$ evaluated at $u=1$ is equal to $4n^2$. Hence, as before, when $\bar{\nu}^2\to 1$ and the ratio of mode frequency to depressed transverse frequency approaches from above the uppermost resonance, $\omega_n/\omega=\pm 2n$, the coefficient which multiples the mode amplitude, $(1-\bar{\nu}^2)/\bar{\nu}^2$, approaches zero.

4. Test ions with nonzero angular momentum

As a simple example for particles with nonzero angular momentum $\bar{P}_\theta\neq 0$, we consider perturbations around an interior circular orbit with constant radius $\bar{r}_c=r_c/R_0$. Assuming $\delta\psi=0$, the value of angular momentum which is consistent with this unperturbed circular motion is easily found from Eq. (19) by imposing the condition $\bar{r}_c=\text{const}$. This gives

$$\left(\kappa-\frac{K}{R_0^2}\right)\bar{r}_c-\frac{\bar{P}_\theta^2}{\bar{r}_c^3}=0, \tag{41}$$

which has the solution $\bar{P}_\theta^2=\bar{r}_c^{\,4}\kappa\bar{\nu}^2$.

For a given value of $\bar{P}_\theta^2$, the particle motion in the equilibrium orbit is purely azimuthal with constant radius $\bar{r}_c$. The frequency of motion around this circular orbit is $\omega^2=\kappa\bar{\nu}^2$. If, however, the ion is perturbed radially slightly away from the equilibrium, the trajectory will consist of small radial oscillations about $\bar{r}=\bar{r}_c$. (This also holds for a small perturbation in the azimuthal direction, which is equivalent to a small change in $\bar{P}_\theta^2$, and hence in the equilibrium radius.) These small radial deviations oscillate with a frequency different from the azimuthal motion: we expect from dynamical considerations that the frequency of small radial deviations ω_c will be twice the frequency of azimuthal motion ω, and this can be verified by direct calculation. Using the equilibrium angular momentum found from Eq. (41), we linearize Eq. (21) for small perturbations $\delta\bar{r}$ about the orbit $\bar{r}=\bar{r}_c$. The linearized equation of motion for the perturbed radius $\delta\bar{r}=\bar{r}-\bar{r}_c$ with no collective modes present is $\delta\bar{r}''+4\kappa\bar{\nu}^2\delta\bar{r}=0$, and hence the frequency of small radial oscillations about this circular orbit is found to be

$$\omega_c^2=4\kappa\bar{\nu}^2. \tag{42}$$

The perturbed radial frequency ω_c is indeed twice the equilibrium azimuthal frequency, and is furthermore independent of the equilibrium radius $\bar{r}_c$. If these small radial orbit deviations resonate with the collective mode, oscillating with independent eigenfrequency ω_n, the particle will experience an energy change. The radial deviations, for example, may cause the perturbed particle trajectory to be outside the equilibrium circle $\bar{r}_c$ when the electrostatic collective mode perturbation is decreasing towards the edge of the beam, and inside the equilibrium circle when the reverse occurs. (See Fig. 3.)

We now consider in particular the linearization of Eq. (27), the equation of motion in a beam supporting an $n=1$ collective mode, for small perturbations $\delta\bar{r}$ away from an equilibrium circle $\bar{r}_c$ such that $\delta\bar{r}=\bar{r}-\bar{r}_c$. The equation takes the form $\delta\bar{r}''+\omega_c^2\delta\bar{r}-\delta_1(\omega_0^2-\omega^2)(\delta\bar{r}+\bar{r}_c)\cos\omega_1 s=0$, which is again a Mathieu-type equation, now both parametrically and externally driven. The frequency of the $n=1$ collective mode is given by $\omega_1^2=\kappa(2+2\bar{\nu}^2),$ and therefore the ratio of the frequencies is

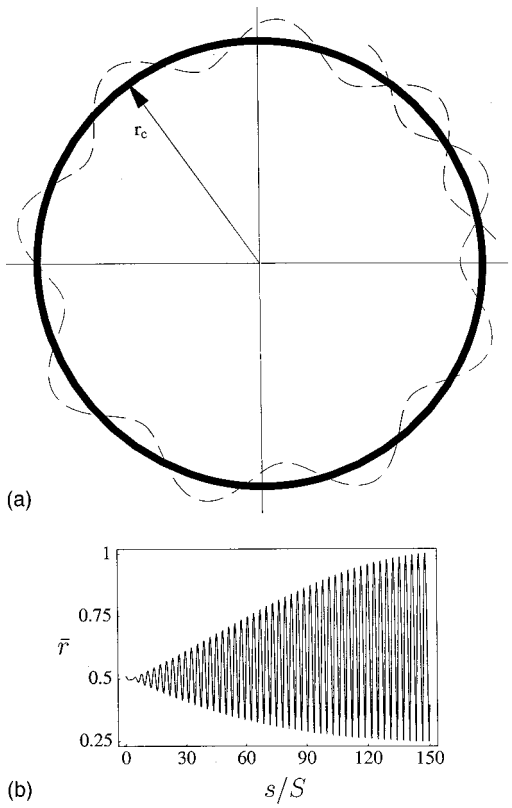

FIG. 3. Representative perturbation about a circular orbit: (a) the oscillations in and out of the reference orbit may resonate with the collective mode, and (b) cause test ion energy gain. The beam parameters in (b) are $\bar{\nu}^2\simeq 0.95$ and $\Gamma=2.5\%$.

$$\frac{\omega_1^2}{\omega_c^2}=\frac{2+2\bar{\nu}^2}{4\bar{\nu}^2}. \tag{43}$$

The ratio in Eq. (43) is equal to unity (fundamental resonance) for $\bar{\nu}^2=1$. In addition, there is no nonlinear frequency shift in the radial oscillation about the equilibrium orbit. Therefore, for $\bar{\nu}^2\simeq 1$, perturbed radial oscillations may grow in amplitude by being in phase with the collective mode. That is, the particle motion may be outside the equilibrium circular orbit $\bar{r}_c$ when the quadratic $n=1$ mode potential is decreasing with radius, and inside the equilibrium circle one half period later when the collective mode is increasing with radius. Two effects will limit this energy gain. First, when the particle orbit grows sufficiently large, it will encounter the finite beam radius, and sample the nonlinear fields in the exterior of the beam, leading to rapid frequency detuning and subsequent energy loss. Second, as mentioned above, the collective mode is multipled by a coefficient proportional to $1-\bar{\nu}^2$. Since the fundamental resonance $\omega_c=\omega_1$ occurs at $\bar{\nu}^2=1$, energy gain must occur near resonance, but before the coefficient cuts off the mode. Therefore, the small detuning away from resonance necessitated by the coefficient $1-\bar{\nu}^2$ will lead to eventual stability of the particle orbit. Figure 3

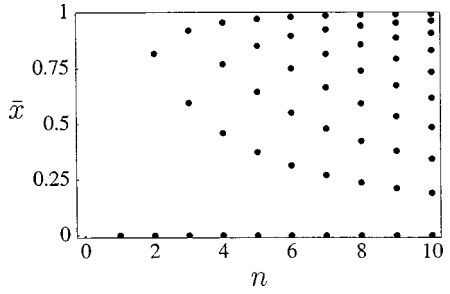

FIG. 4. Radial location $\overline{\rho}_n^i(\overline{x})$ of nodes as a function of mode number n.

illustrates a test ion trajectory being expelled from deep within the beam near the fundamental resonance. The beam is tenuous, with space-charge depression factor of $\overline{\nu}^2 \simeq 0.95$.

B. Nonresonant behavior

We now consider the effects of nonresonant energy changes on the test particle dynamics. Since the particle can only gain a limited amount of energy before giving it back, nonresonant trajectory changes, while they may have an effect on beam emittance, will dramatically affect the single-particle dynamics only if the mode causes the particle to sample both the beam interior and the exterior region when it normally would not, and thus is only of interest for particles with energy ''close'' to the escape energy from the beam core.

We treat explicitly the $n=2$ collective mode: the $n=1$ mode can be included as a special case. From numerical test ion studies, the $n=1$ and $n=2$ modes appear to be the most likely to expel significant numbers of particles. In the equation describing the test ion trajectory in the beam interior, Eq. (21), the polynomial $(\partial/\partial\overline{r})\delta\psi_n(\overline{r})$ generally has n nodes $\{\overline{\rho}_n^1,\ldots,\overline{\rho}_n^n\}$ in the interior. At these nodes, the value of the perturbed radial self-field always vanishes, as alluded to in Eq. (36). (See Fig. 4.) It is difficult for particles whose equilibrium trajectories achieve a maximum radius $\overline{r}_0<\overline{\rho}_n^i$ to gain enough energy to exceed the radius $\overline{\rho}_n^i$. As the particle gains energy and is pushed towards $\overline{\rho}_n^i$, the parametric driving term approaches zero, thereby cutting off the energy gain. This increasing density of nodes stratifies the beam into ''zones'' between nodes, preventing all but those test ions sampling the outermost zone from gaining sufficient energy to be expelled. In addition, from Fig. 4 it is clear that the outermost zone $(\overline{\rho}_n^n,1)$, between the last node and the beam radius $\overline{r}=1$, shrinks to zero thickness as n increases and $\overline{\rho}_n^n \to 1$. The $n=1$ and $n=2$ collective modes have the largest zones capable of expelling particles easily from the beam.

The perturbation treatment consists of finding a transformation which pushes the perturbations in the Hamiltonian to higher order, which can then be neglected, leaving an integrable, approximate, lower-order Hamiltonian [20]. This simpler system will then be used to estimate the range of normally confined particles inside the beam edge which can sample the highly nonlinear region exterior to the beam.

The one-dimensional nonautonomous Hamiltonian for the beam *interior*, $H(\overline{x},\overline{p},s)$, is defined in Eq. (37), where $\overline{p}$ denotes $d\overline{x}/ds$. The position and momentum are transformed into action-angle form to prepare the Hamiltonian for canonical perturbation theory. The action J, invariant in the unperturbed case, and the angle θ, linearly advancing in the unperturbed case, are related to the original coordinates by

$$\overline{x} \doteq (2J/\omega)^{1/2}\sin\theta, \qquad \overline{p} \doteq (2J\omega)^{1/2}\cos\theta, \tag{44}$$

and the equilibrium trajectories in (J,θ) space are straight lines with

$$J=\text{const}, \qquad \theta=\omega s+\theta_0. \tag{45}$$

The canonically transformed Hamiltonian, $\mathcal{H}(J,\theta,s) = H(\overline{x},\overline{p},s)$, with $\epsilon=\delta_2(\omega_0^2-\omega^2)$, is given by

$$\mathcal{H}=\omega J-\epsilon\left[\left(\frac{J}{\omega}\right)\sin^2\theta-\frac{3}{2}\left(\frac{J}{\omega}\right)^2\sin^4\theta\right]\cos\omega_2 s. \tag{46}$$

Using standard perturbation theory [20], we express $\mathcal{H} \simeq \mathcal{H}_0+\epsilon\mathcal{H}_1$ and let $S\simeq\tilde{J}\theta+\epsilon S_1$ generate the near-identity transformations

$$J=\frac{\partial S}{\partial\theta}\simeq\tilde{J}+\epsilon\frac{\partial S_1}{\partial\theta}, \qquad \tilde{\theta}=\frac{\partial S}{\partial\tilde{J}}\simeq\theta+\epsilon\frac{\partial S_1}{\partial\tilde{J}}. \tag{47}$$

We further assume a canonical transformation, $\tilde{\mathcal{H}}(\tilde{J},\tilde{\theta}) = \mathcal{H}(J,\theta)$, and expand about the small change in (J,θ). This gives

$$\tilde{\mathcal{H}}(\tilde{J},\tilde{\theta})=\mathcal{H}_0(\tilde{J})+\epsilon\mathcal{H}_1(\tilde{J},\tilde{\theta})+\epsilon\frac{\partial S_1}{\partial\tilde{\theta}}\frac{\partial\mathcal{H}_0}{\partial\tilde{J}}. \tag{48}$$

Note that $\partial\mathcal{H}_0/\partial\tilde{J}=\omega(\tilde{J})$. Separating the perturbed quantities into constant $\langle\cdot\rangle$ and fluctuating $\{\cdot\}$ portions, the assumption that the fluctuations are higher order requires that we choose S_1 to cancel the fluctuations to this order, which gives

$$\frac{\partial S_1}{\partial s}+\omega\frac{\partial S_1}{\partial\tilde{\theta}}=-\{\mathcal{H}_1\}. \tag{49}$$

When we Fourier expand S_1 and $\mathcal{H}_1$ in the timelike variable s, this gives for S_1

$$S_1=\sum_{(l,m)\neq(0,0)}S_1^{l,m}=\sum\ i\frac{\mathcal{H}_1^{l,m}(\tilde{J})}{l\omega(\tilde{J})+m\omega_2}\exp\{i(l\tilde{\theta}+m\omega_2 s)\}, \tag{50}$$

where the individual $\mathcal{H}_1^{l,m}$ components are defined by

$$2\mathcal{H}_1^{0,\pm 1}=\frac{1}{2}\frac{J}{\omega}-\frac{2}{10}\frac{J^2}{\omega^2},$$

$$2\mathcal{H}_1^{2,\pm 1}=-\frac{1}{4}\frac{J}{\omega}+\frac{3}{4}\frac{J^2}{\omega^2}, \tag{51}$$

$$2\mathcal{H}_1^{4,\pm 1}=-\frac{3}{32}\frac{J^2}{\omega^2}.$$

Since the perturbation in H has a vanishing average, there is no constant $\mathcal{H}_1^{0,0}$ term, and the perturbed frequency remains unchanged to this, or any, order. In addition, Eqs. (50) and (51) show clearly the resonances at $\omega_2/\omega=\pm 2,4$ discussed in Sec. III A 2.

The new invariant $\tilde{J}$ is given by the transformations in Eq. (47),

$$\tilde{J}(J,\theta,s)=J+\epsilon J_1=J-\epsilon\partial_s S_1=J-\epsilon\sum\, ilS_1^{l,m}, \tag{52}$$

and J_1 is found to be

$$\begin{aligned}J_1=2\mathcal{H}_1^{2,1}\Bigg(&\frac{\exp\{i(2\tilde{\theta}+\omega_2 s)\}}{2\omega+\omega_2}+\frac{\exp[i(-2\tilde{\theta}-\omega_2 s)]}{-2\omega-\omega_2}\\&+\frac{\exp\{i(2\tilde{\theta}-\omega_2 s)\}}{2\omega-\omega_2}+\frac{\exp\{i(-2\tilde{\theta}+\omega_2 a)\}}{-2\omega+\omega_2}\Bigg)\\&+4\mathcal{H}_1^{4,1}\Bigg(\frac{\exp\{i(4\tilde{\theta}+\omega_2 s)\}}{4\omega+\omega_2}+\frac{\exp\{i(-4\tilde{\theta}-\omega_2 s)\}}{-4\omega-\omega_2}\\&+\frac{\exp\{i(4\tilde{\theta}-\omega_2 s)\}}{4\omega-\omega_2}+\frac{\exp\{i(-4\tilde{\theta}+\omega_2 s)\}}{-4\omega+\omega_2}\Bigg).\end{aligned} \tag{53}$$

In Eq. (53) we may approximate $\tilde{\theta}$ by the unperturbed angle orbit, $\tilde{\theta}\simeq\theta=\omega s+\theta_0$, and the error will appear only in J_2. The expression for $\tilde{\theta}$ correct to first order may be obtained from the transformations in Eq. (47) and the expression for S_1 in Eq. (50), but this is less important for our purposes here. We define the ratio of the frequencies of the $n=2$ mode and the depressed transverse oscillation frequency to be $\alpha=\omega_2/\omega$. Expressing the exponentials in terms of trigonometric functions, Eq. (53) reduces to

$$\begin{aligned}J_1=2\mathcal{H}_1^{2,1}\Bigg(&\frac{2}{\omega(2+\alpha)}\sin[(2+\alpha)\omega s]+\frac{2}{\omega(2-\alpha)}\\&\times\sin[(2-\alpha)\omega s]\Bigg)+4\mathcal{H}_1^{4,1}\Bigg(\frac{2}{\omega(4+\alpha)}\\&\times\sin[(4+\alpha)\omega s]+\frac{2}{\omega(4-\alpha)}\sin[(4-\alpha)\omega s]\Bigg).\end{aligned} \tag{54}$$

With appropriate phase adjustments to account for initial conditions, the new invariant $\tilde{J}(J,s)$ in Eq. (52) is numerically verified to be conserved to within a few percent. This small fluctuating error can be accounted for in higher orders.

The perturbed orbit in the physical coordinates $(\bar{x},\bar{p})$ is given from Eq. (44) by $\bar{x}(s)=\sqrt{2\tilde{J}(s)/\omega}\sin\tilde{\theta}(s)$. By assuming that $\tilde{J}(s)$ and $\sin\tilde{\theta}(s)$ can be maximized independently, the maximum value of $\tilde{J}(s)$, which we denote by $\tilde{J}^*$, thus places an absolute upper bound on the trajectory excursion. The largest radial excursion $\bar{x}^*$ by this estimate is

$$\bar{x}^*=\sqrt{\frac{2\tilde{J}^*}{\omega}}. \tag{55}$$

Here $\tilde{J}^*=J+\epsilon J_1^*$ from Eq. (52), where J_1^* is the maximum of Eq. (54). If the ratio of frequencies α is irrational, then J_1 in Eq. (54) eventually passes arbitrarily close to the limiting value

$$\begin{aligned}J_1^*=2\mathcal{H}_1^{2,1}\Bigg(&\frac{-2}{\omega(2+\alpha)}+\frac{2}{\omega(2-\alpha)}\Bigg)+4\mathcal{H}_1^{4,1}\Bigg(\frac{-2}{\omega(4+\alpha)}\\&+\frac{2}{\omega(4-\alpha)}\Bigg).\end{aligned} \tag{56}$$

Equations (55) and (56) constitute a simple estimate of the maximum interior radial excursion of test ions when launched with different initial actions, and hence different initial radii, consistent with Eq. (44). In practice, the complicated interdependence of $\tilde{J}$ and $\bar{\theta}$ on the unperturbed action and time (J, s) makes Eq. (55) an overestimate, although Eq. (56) is numerically found to be very accurate. Small numerical coefficients to make the theory more accurate will be discussed in Sec. IV. Other complications are considered in Appendix A.

The estimation in Eq. (55) of the maximum excursion of a test ion in a beam perturbed with collective modes provides a simple way to make a guess at the time scale for a test particle to move to the orbit farthest from its equilibrium trajectory. It was assumed in simplifying Eq. (54) to obtain Eq. (56) that the terms with frequencies $(2+\alpha)\omega,(2-\alpha)\omega,\ldots$ would eventually constructively interfere. (Recall that α is the ratio of the collective mode frequency to the depressed particle transverse frequency.) The time scale for a particle to maximize its energy gain, and possibly move out of the beam, can be estimated by judiciously choosing a rational number m/n near $(2+\alpha)/(2-\alpha)$. The time scale is then on the order of mT_-, where $T_-=2\pi/(2-\alpha)\omega$. This provides a fairly accurate estimate for particles inside the beam, provided m and n are selected without demanding that $(2+\alpha)/(2-\alpha)$ match m/n too precisely.

We now apply the estimate of maximum trajectory excursions, Eq. (55), to calculating which particles near the edge of the beam will gain enough energy to leave the beam core at some point in their trajectory. The most important parameter in this investigation is $\epsilon=\delta_2(\omega_0^2-\omega^2)$, the strength of the $n=2$ collective mode. The objective is to find the radial value $\bar{x}_S$ at which a particle, launched with initial energy equivalent to an unperturbed maximum radius $\tilde{x}_0$, gains enough energy to just reach the beam edge. [Launching particles with zero initial radial velocity, which we assume is

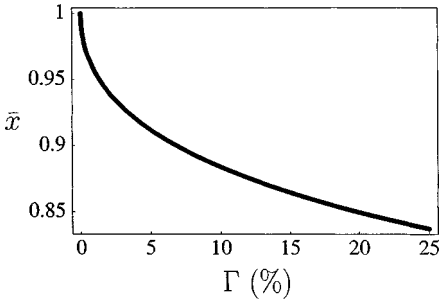

FIG. 5. Plot of $\overline{x_S}$ as a function of Γ (in %) for $\overline{\nu^2}=1/4$.

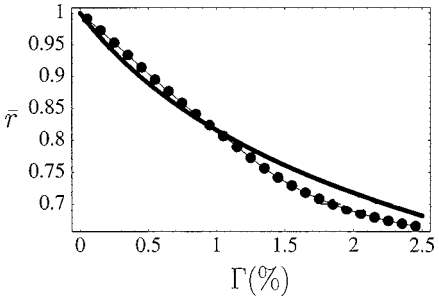

FIG. 6. Comparison of adjusted analytical prediction (solid line) and numerical solutions (dotted line) of the minimum radius for expulsion. Plot of $\overline{x_S}$ versus Γ (in %).

the case, makes the initial radial value $\overline{x_0}$ equal to the maximum unperturbed value, and implies $J=1/2\omega\overline{x}^2$, from Eq. (44).] We call $\overline{x_S}$ the *stripping radius*. That is, the maximum excursion $\overline{x}^*$ is a function of $\overline{x_0}$, and $\overline{x_0}=\overline{x_S}$ is defined by

$$\overline{x}^*(\overline{x_S})=1, \tag{57}$$

or equivalently, $x^*(x_S)=R_0$. Particles with maximum unperturbed radius $\overline{x_0}>\overline{x_S}$ are able to sample the region exterior to the beam—at which point the Hamiltonian in Eq. (37) becomes invalid—even though $\overline{x_0}<1$, and thus have their motion partially described by Eq. (26), valid for $\overline{x}>1$. Once sampling the highly nonlinear exterior region, the particles have the potential for large energy gains. These energy gains are explored in Sec. IV. Particles with smaller energies will nonresonantly gain energy and then give it up.

To find this minimum radius for expulsion, Eq. (57) is substituted in Eq. (55), where we evaluate $\tilde{J}^*$ in Eq. (56) at $\tilde{x}_S$ using, $J\to 1/2\omega\overline{x}_S^2$. The result of some simple algebra is

$$\overline{x}_s^2=\frac{-(1+\epsilon d_2)\pm[(1+\epsilon d_2)^2+2\epsilon d_1\omega]^{1/2}}{\epsilon\omega d_1}. \tag{58}$$

The constants d_1 and d_2 in Eq. (58) depend only on the depressed transverse frequency and the $n=2$ mode frequency, which in turn depend only on $\overline{\nu}$, and are defined by $d_1=d_3(21\alpha-3/4\alpha^3)$ and $d_2=d_3\omega(-16\alpha+\alpha^3)$, where $d_3^{-1}=\omega^3(64-20\alpha^2+\alpha^4)$, and $\alpha=\omega_2/\omega$. Equation (58) by itself is not sufficiently accurate, but with the small numerical adjustments discussed in Sec. IV A, it gives, within a few percent accuracy over a wide range of parameters, the radial extent of the region near the beam edge from which particles will be ejected from the beam. Equation (58) can be converted from being a function of the small parameter ϵ to a function of $\delta_2^2=\Gamma$, the ratio of the rms electrostatic energies in the mode and in the beam core, using $\epsilon=\delta_2(\omega_0^2-\omega^2)$. Figure 5 shows a plot of $\overline{x_S}$ as a function of δ_2^2, calculated from Eq. (58) without numerical adjustments. The range of particles which sample the beam exterior is of course zero with vanishing mode strength, and constitutes approximately 20% of the beam transverse cross section when $\Gamma=0.05$ (so that the energy in the perturbative mode is about 5% of the energy in the beam equilibrium).

IV. NUMERICAL RESULTS

A. Numerical correction factors for ejection radius estimate

In order to make Eq. (58) more useful, we insert the small (compared to unity) factors $\{\lambda_1,\lambda_2,\lambda_3\}$ according to

$$\overline{x}_S^2=\frac{-[1+\epsilon(1+\lambda_1)d_2]\pm\{[1+\epsilon(1+\lambda_2)d_2]^2+2\epsilon(1+\lambda_3)d_1\omega\}^{1/2}}{\epsilon\omega d_1}. \tag{59}$$

To ensure that the analytical prediction retains the property that no particles are expelled when there is no collective mode, we require that the expression for $\overline{x}_S^2$ approaches unity as ϵ vanishes. We expand for small ϵ and set the coefficient independent of ϵ equal to unity: this implies that $\lambda_2=-\lambda_1$ and $\lambda_3=4/3\lambda_1$. When the coefficients $\{\lambda_i\}$ are small compared to unity, Eq. (59) is a small adjustment to Eq. (58).

A typical plot comparing numerical solutions of the test equations for the unperturbed initial radius of particles just excited to the beam edge and the analytical-numerical prediction, for $\lambda_1\simeq 0.2$, is given in Fig. 6. The overall rate of growth of the range of expulsion is captured by Fig. 6, even if the details (linear initial growth) are not.

B. Comparison of $n=1$ mode and envelope mismatch

Test ion behavior under the influence of an $n=1$ collective mode and a linearized envelope mismatch are distinguished in practice solely by the definitions of ''inside'' and ''outside'' the beam. For $n=1$, inside the beam corresponds to $\{x:x<R_0\}$. For a mismatch, inside the beam corresponds to $\{x:x<R_0(1+\delta_e\cos\omega_e s)\}$, or, more accurately, $\{x:x<R(s)\}$, where $R(s)$ is the exact solution to the envelope equation Eq. (4). (In addition, the mismatch frequency ω_e depends on the amplitude for large mismatches, while the $n=1$ frequency ω_1 does not.)

Since, as mentioned in Sec. III A, the beam boundary in phase space is an invariant torus for the (fully nonlinear)

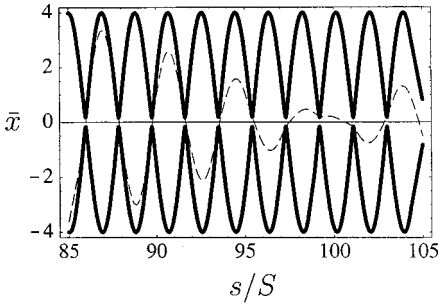

FIG. 7. Indefinitely confined test ion trajectory (light line) inside a beam (dark line) launched at four times the rms-matched value R_{rms}. The beam waist is approximately $0.15R_{\mathrm{rms}}$.

mismatch, whereas it is not for the $n=1$ mode, the behavior of test ions can differ dramatically in the two cases. As an indication of this, Fig. 7 shows that even for very large *mismatches* of the beam edge, particles initially confined inside the beam energy surface remain confined for all time. [This is only true using the fully nonlinear envelope equation Eq. (4) to determine the evolution of $R(s)$ in the test ion equation of motion Eq. (24). See Appendix B.]

For the $n=1$ *collective mode*, however, interior particles can easily escape the beam. Figure 8 shows the maximum excursion as a function of mode amplitude of a test particle launched at $\overline{x_0}=0.95$. The particle is expelled from the beam interior at low mode amplitudes, and can gain substantial energy at higher amplitudes.

C. Maximum excursion

In addition to having worse confinement properties, the collective modes facilitate energy gain by halo particles already outside the beam much more than the envelope mismatch, linearized or not. Particles that start outside of a beam with an envelope ripple gain very little energy [11] due to densely packed KAM surfaces in the region of phase space exterior to the beam. This is true, with full nonlinear mismatch effects, even for very large mismatches, measured by the envelope mismatch parameter, the ratio of maximum beam radius to rms radius, Δ_e. (For small mismatches, $\Delta_e \simeq 1/2\delta_e$.) The collective modes, however, are very conducive to energy gain due to KAM curve breakup in the region exterior to the beam's phase space. In one-dimensional nonautonamous dynamical systems, a phase space spanning curve (KAM curve) forms a boundary to motion and energy gain, and corresponds to an integral of the motion. As parameters are varied, these curves can come into and go out of existence, leading to dramatically different trajectory behavior. If a KAM curve is destroyed, a particle trajectory can stochastically explore a large region of phase space, corresponding gaining more energy and larger maximum excursion. Figure 9 shows the phase space structure for a small envelope mismatch and an $n=1$ mode with an equal amount of electrostatic energy. The limitations to energy gain outside the fully nonlinear mismatched beam are evident from this Poincaré plot, and the lack of limitations for the $n=1$ mode, are contrasted in Fig. 10. For the former, a KAM curve clearly constrains a particle with initial radius $\overline{x_0}=1.1$ to negligible energy gain for very large mismatch parameter, $\Delta_e \simeq 1.3$. For the latter, the maximum excursion of test ions increases rapidly with mode amplitude, particularly as KAM surfaces are destabilized.

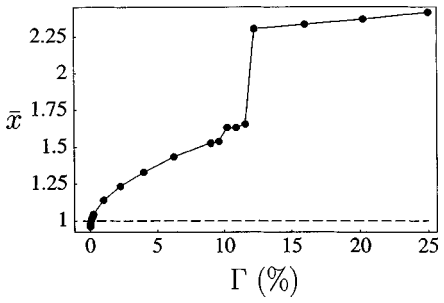

FIG. 8. Plot of the maximum excursion of a test particle as a function of mode energy Γ (in %). The test ion was launched at $\overline{x}=0.95$. The dashed line is the beam edge at $\overline{R}=1$.

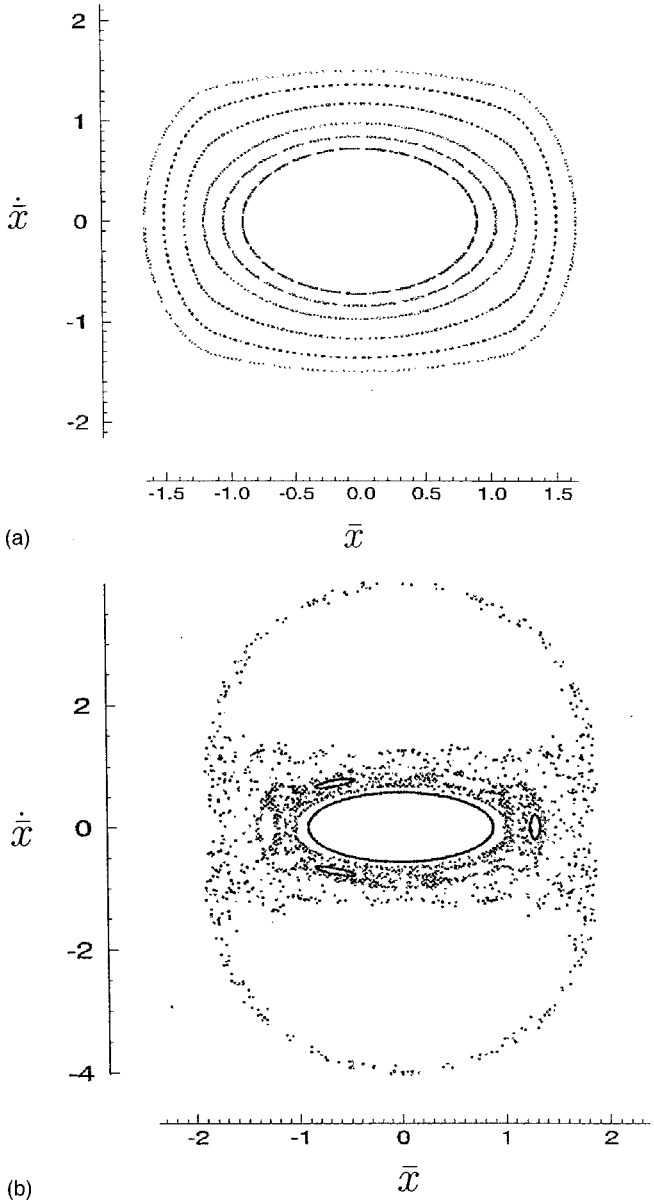

FIG. 9. Phase space structures for two differing perturbations: (a) mismatched beam with no other perturbations, and (b) $n=1$ collective mode. Both perturbations have rms electrostatic energies which are 5% of the beam core energy.

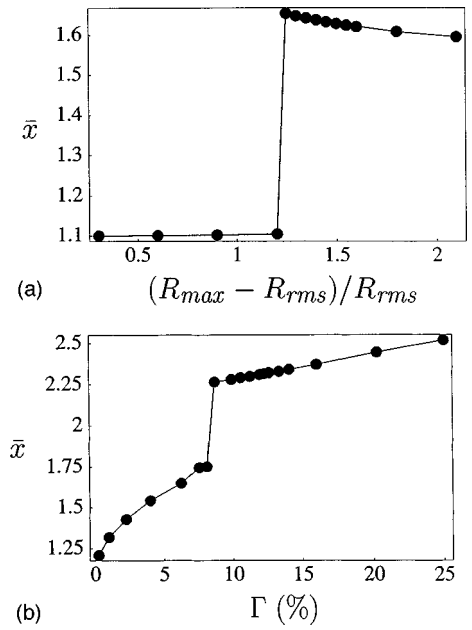

FIG. 10. Maximum excursion of a test ion versus relative rms energy for two different perturbations with $\bar{\nu}^2 = 1/3$. The two cases correspond to (a) mismatched envelope (the jump corresponds to a large mismatch parameter of $R_0 \simeq 2.3 R_{\rm rms}$), and (b) $n=1$ collective mode.

Particles whose energy corresponds to a maximum unperturbed trajectory, which we denote $\bar{x}_0$, between $\bar{x}_\Delta$ and 1, will be ejected by the collective modes from the beam at some point, with the possibility of large energy gains. In general, ejected particles either (i) experience negligible energy gains, or (ii) obtain a well-defined maximum excursion $\bar{X}_1 \simeq 1.5$. This behavior is a function of space-charge depression $\bar{\nu}$, rms field energy in the nth mode relative to rms electrostatic energy in the beam core $\Gamma \equiv \mathcal{E}_n/\mathcal{E}_0$, and the ejected particle's unperturbed maximum radius $\bar{x}_0$.

For mode energies less than a certain critical energy $\Gamma_1(\bar{\nu},\bar{x}_0)$, particles travel no further than a few percent of R_0 outside of the beam; for energies greater than Γ_1, particles consistently travel as far out as $\bar{X}_1 \simeq 1.5$ (see Fig. 11). The value of Γ_1 decreases as the beam becomes more intense, ranging from less than 2% at $\bar{\nu}^2 = 1/5$ to 15% at $\bar{\nu}^2 = 1/2$. (See Fig. 12.) In addition, particles with $\bar{x}_0$ further from the beam edge have higher critical energies, and of course particles with $\bar{x}_0 < \bar{x}_\Delta$ never leave the beam. The value of $\bar{X}_1$ gradually increases with Γ, and depends weakly on $\bar{\nu}$. Since

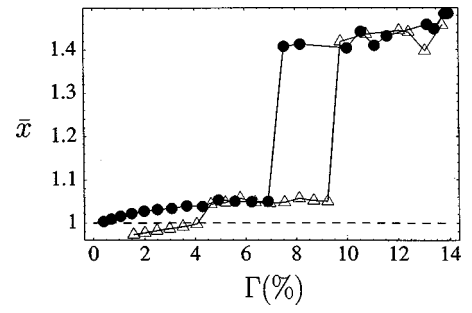

FIG. 11. Plot of $\bar{x}_{\rm max}$ versus Γ (in %) for $\bar{\nu}^2 = 1/3$ with $\bar{x}_0 = 0.99$(●) and $\bar{x}_0 = 0.95$(△).

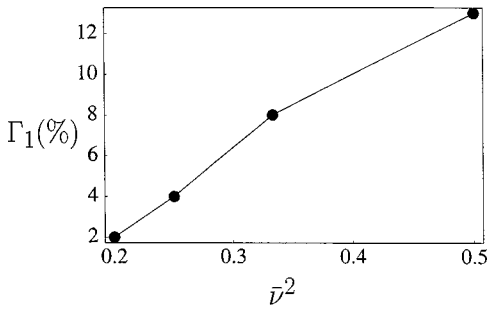

FIG. 12. Plot of first critical energy Γ_1 as a function of space-charge factor $\bar{\nu}$ with $\bar{x}_0 = 0.95$.

$\bar{X}_1$ does not depend on $\bar{x}_0$, this is the largest radius any particle initially in the beam can escape to, and functions as a KAM curve, giving an indication of the phase space structure in the halo region.

Finally, for intense beams with sufficiently large amplitude modes, this phase-space spanning curve can be destabilized and broken into islands. Above a critical energy Γ_2, particles can explore out to $\bar{X}_2 \simeq 2$ (see Fig. 13). It is plausible that, for extremely intense beams, larger collective mode amplitudes would make accessible even greater regions of phase space.

V. CONCLUSIONS AND FUTURE WORK

This paper has presented a method of halo formation based on collective mode excitations, providing possible processes both for expelling particles from the beam core and a means of accelerating particles once they are able to sample the exterior region.

Collective modes using the fluid model of Lund and Davidson [15] allow the derivation of test ion equations of motion in the beam interior and exterior regions. The behavior of particles which remain interior to the beam can be analyzed theoretically, and we have calculated perturbed orbits for particles subject to $n=1$ and 2 mode perturbations. This provides estimates regarding the range of initial conditions for which particles will be expelled from the beam. Resonances for meridional particles are found to be unimportant, while a class of particles with nonzero angular momentum are found to participate in resonant behavior.

Once expelled from the beam, numerical methods are required, which indicate that KAM curves confine particles within 1.5 times the beam radius for moderately low mode amplitudes, but are successively destabilized for higher amplitudes.

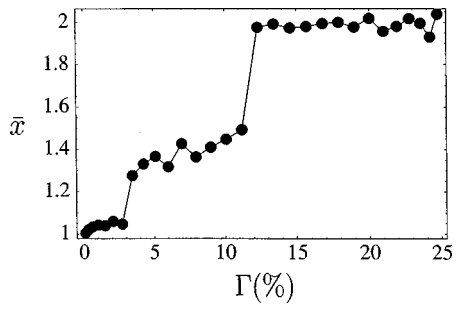

FIG. 13. Plot of $\bar{x}_{\rm max}$ versus Γ (in %) for $\bar{\nu}^2 = 1/5$.

An issue which remains to be explored is the time scale over which particles are ejected from the beam and gain significant energy. While collective modes have the potential to affect large classes of particles, if the energy gain occurs slowly compared to other expulsive processes, or if it occurs slowly enough to be easily remedied by collimation, collective modes may not be a serious concern.

It appears difficult to estimate the time scale for expulsion analytically. While the discussion in Sec. III B of the approximate time to maximize a test ion's energy gain provides a useful measure for the expulsion of test particles inside the beam, particle acceleration to high energies once *outside* the beam is also an important issue. The acceleration of such tail particles can only be estimated numerically.

In addition, the sensitivity of the particle dynamics to the various assumptions made in the model is a subject for future study. While space-charge dominated beams are nearly uniform in density out to the beam radius R, after which the beam density falls abruptly to zero, a small region within a few Debye lengths at the beam edge has a highly nonuniform density, and hence nonlinear fields. Several authors [9] have noted the effects of including the abrupt falloff at the beam edge. Initial numerical simulations which replace the sharp beam edge with a falloff over a short but finite distance, assuming the same form for the collective modes, indicate that the effect is not significant on the main features of particle behavior found in Poincaré plots. Another important assumption in the model is the smooth-focusing approximation: although the functional forms for finite bunch collective modes have been derived [21], it is uncertain what affect using these more realistic periodic-focusing models would have on the present results. Recent numerical work by Gluckstern *et al.* [22] indicates that three-dimensional bunch dynamics play an important role in halo formation.

ACKNOWLEDGMENTS

This work was supported by the Department of Energy and in part by the Office of Naval Research.

APPENDIX A: COMPLICATIONS IN THE ANALYTICAL ESTIMATE

Equations (55) and (56) form an analytical estimate of the radial extent of the region from which particles will be ejected from the beam. It is unsatisfactory for several reasons. Equation (55) is based upon the assumption that $\tilde{J}(s)$ and $\sin\tilde{\theta}(s)$ can be independently maximized, but this is impossible because of the Hamiltonian constraint of area preservation. The new action and angle generated by the near-identity transformations in Eq. (47) are individually quite accurate and are separately easy to maximize. It is difficult using elementary techniques, however, to determine the maximum excursion in the original radial variable, $\overline{x(s)} = \sqrt{2\overline{J}(s)/\omega}\sin\tilde{\theta}(s)$. This is due to the fact that $\overline{J}$ and $\overline{\theta}$ depend in a complicated way on the timelike coordinate s. The $\tilde{J}$ dependence is given in Eqs. (54) and (52). The $\tilde{\theta}$ dependence can be determined from Eq. (47), and has a similar form. The value $\overline{x(s)}$ then takes the schematic form $\overline{x} = f(s)\sin g(s)$ where $f(s)$ and $g(s)$ each have trigonometric terms with $2n$ frequencies for the nth collective model. It is difficult to reliably maximize this expression, even using Bessel-like expansions of the $\sin g(s)$ term. Indeed, the maximum excursion behaves in a sufficiently complicated way that it is unlikely that any simple analytical approximation will capture all relevant behavior. This difficulty in maximizing the expressions is therefore handled by introducing the numerical coefficients in Sec. IV A.

In addition, in the method used here, the fact that particles approach close to the only nonzero node for the $n=2$ collective mode, $\overline{\rho}_2^1 = \sqrt{2/3}$, but no further, is contained in this interdependence. That is, the ''interference'' between $\tilde{J}^*(s)$ and $\tilde{\theta}(s)$ not only makes Eq. (55) an overestimate, but makes the maximum radial excursion as a function of initial energy behave in a complicated fashion near the nodes. Away from the node, at the beam edge, the numerical factors can account for this overestimate.

Another complication is the violation of the assumption that the the mode oscillation is fast compared to the transverse trajectory oscillation. Although this holds over the entire oscillation, the mode may not oscillate quickly enough for the force to average to zero over a particular section of the trajectory. In particular, the test ion, between passing the node $\overline{\rho}_2^2 = \sqrt{2/3}$ and reaching its maximum excursion, may experience a force of the same sign. The Hamiltonian method above would require interference from higher order harmonics to accurately approximate this force which appears quasisteady on a short time scale. The result is that particle trajectories in a sufficiently slow collective mode, relative to the transverse oscillation, have their energy gain temporarily underestimated, and can move out of the beam more easily than analytically predicted. To estimate when this happens, we compare the time T_ρ between a typical unperturbed test ion's passing the node $\overline{\rho}_2^2$ and reaching its maximum unperturbed excursion halfway between the node and the beam edge, and a collective mode half-period $1/2T_2$. We find that a test ion will experience a force averaging to zero when $\overline{\nu} \ll 0.25$. Numerical studies confirm that, under the opposite condition $\overline{\nu} > 0.25$, moderate amplitude modes can expel particles from the beam almost immediately once they are able to pass the node.

APPENDIX B: USE OF THE LINEARIZED ENVELOPE EQUATION

The statement that interior particles are confined for all time in an envelope mismatch is only true using the fully nonlinear envelope equation Eq. (4) in the test ion equation of motion Eq. (24). Since the expansion $R(s) = R_0(1 + 1/2\,\delta_\epsilon \cos\omega_\epsilon s)$ is near the beam edge for small initial disturbances from the matched radius, this expansion is ''almost'' an energy surface. Where it is a valid expansion, particles may travel a small distance out of the beam, but do not gain a significant amount of energy. If the linearized expression for the beam envelope is used for large δ_ϵ, particles can experience very large gains. (The exact envelope confines particles for any size mismatch, as is evident from Fig. 7.) Thus, predictably, the linear expansion behaves ''nicely'' for small perturbations, but becomes unphysical for large mismatches even though solutions to the full nonlinear equations continue to be well behaved.

A similar statement might conceivably be made about the linearized collective modes used here, namely, that the deleterious effects are due to using linearized modes in a situation where the full nonlinear perturbative structure would remain well behaved. However, since the appropriate measure of smallness is that the energy in the perturbative modes be small compared to the field energy of the unperturbed beam, it is possible to introduce perturbations on realistic intense beam equilibria which have significant effects on particle behavior despite their small amplitude.

[1] R. C. Davidson, *Physics of Nonneutral Plasmas* (Addison-Wesley, Reading, MA, 1990), and references therein.
[2] M. Reiser, *Theory and Design of Charged-Particle Beams* (Wiley, New York, 1994), and references therein.
[3] *Space Charge Dominated Beams and Applications of High Brightness Beams*, edited by S. Y. Lee, AIP Conf. Proc. No. 377 (AIP, New York, 1996), and references therein.
[4] J. Lagniel, Nucl. Instrum. Methods Phys. Res. A **345**, 46 (1994).
[5] R. Gluckstern, W. Cheng, and H. Ye, Phys. Rev. Lett. **75**, 2835 (1995).
[6] R. Gluckstern, Phys. Rev. Lett. **73**, 1247 (1994).
[7] E. Lee, S. Yu, and W. Barletta, Nucl. Fusion **21**, 961 (1981).
[8] M. Ikegami, Phys. Rev. E **59**, 2330 (1999).
[9] H. Okarnoto and M. Ikegami, Phys. Rev. E **55**, 4694 (1997).
[10] R. Jameson, Fusion Eng. Des. **32–33**, 149 (1996).
[11] R. Pakter and C. Chen (unpublished).
[12] Q. Qian, Ph.D. thesis, Princeton University, 1995 (unpublished); Q. Qian, W. Lee, and R. Davidson, Phys. Plasmas **4**, 1915 (1997).
[13] Y. Fink, C. Chen, and W. Marable, Phys. Rev. E **55**, 7557 (1997).
[14] R. Davidson and C. Chen, Part. Accel. **59**, 175 (1998).
[15] S. Lund and R. C. Davidson, Phys. Plasmas **5**, 3028 (1998).
[16] R. Davidson, W. Lee, and P. Stoltz, Phys. Plasmas **5**, 279 (1998).
[17] R. Gluckstern, in *Proceedings of the 1970 Proton Linear Accelerator Conference*, edited by M. R. Tracy (National Accelerator Laboratory, Batavia, IL, 1971), p. 811.
[18] M. McLachlan, *Theory and Applications of Mathieu Functions* (Dover, New York, 1964).
[19] A. Riabko, M. Eilison, X. Kang, S. Lee, D. Li, J. Liu, X. Pei, and L. Wang, Phys. Rev. E **51**, 3529 (1995).
[20] A. J. Lichtenberg and M. A. Lieberman, *Regular and Chaotic Dynamics*, 2nd ed. (Springer-Verlag, New York, 1992), and references therein.
[21] H. Uhm and M. Lampe, Phys. Fluids **24**, 1553 (1981).
[22] R. Gluckstern, A. Fedetov, S. Kurennoy, and R. Ryne, Phys. Rev. E **58**, 4977 (1998).